Mutation of Asparagine 52 to Glycine Promotes the Alkaline Form of Iso-1-cytochrome *c* and Causes Loss of Cooperativity in Acid Unfolding†

Saritha Baddam and Bruce E. Bowler*

Department of Chemistry and Biochemistry, University of Denver, 2190 East Iliff Avenue, Denver, Colorado 80208-2436

Received December 7, 2005; Revised Manuscript Received February 13, 2006

ABSTRACT: The kinetics and thermodynamics of the alkaline and acid conformational transitions of a Lys 79 → Ala/Asn 52 → Gly (A79G52) variant of iso-1-cytochrome *c* are studied. The Lys 79 → Ala mutation is designed to limit heme ligation in the alkaline conformer to Lys 73. The Asn 52 → Gly mutation is intended to shift the population of the alkaline conformer to physiological pH based on the hierarchical nature of the cooperative substructures of this protein. The midpoint pH for formation of the alkaline conformer is ∼7.45. The kinetics for the alkaline conformational transition of the A79G52 variant are consistent with the ionization constant, pK_H, for the trigger group controlling formation of the alkaline conformer being ∼9.5. This pK_H is low for alkaline conformers involving lysine−heme ligation but is consistent with the pK_a of the highest of three ionizable groups which modulate formation of the histidine−heme alkaline conformer of a His 73 variant of iso-1-cytochrome *c* [Martinez, R. E., and Bowler, B. E. (2004) *J. Am. Chem. Soc. 126,* 6751−6758]. The acid transition of the A79G52 variant is split into two phases. Both the Lys 79 → Ala and Asn 52 → Gly mutations are expected to affect the buried hydrogen bond network of cytochrome *c,* suggesting that this network is an important modulator of the acid unfolding of cytochrome *c*.

Mitochondrial cytochrome *c* has long been known to undergo a series of pH-dependent conformational changes (*1*). In the oxidized form of the protein, five states have been recognized, with the native state of the protein (state III) being populated near neutral pH:

Ferricytochrome *c* State:	I →	II →	III →	IV →	V
pK (horse heart protein):	0.4	2.5	9.35	12.8	

The acid (state III to II) and the alkaline (state III to IV) transitions of cytochrome *c* have been of particular interest. The acid transition typically occurs near pH 2.5 (*2*) and is a multiproton process (two to three protons). The alkaline transition, on the other hand, is a one-proton process with a midpoint p*K* that varies from 7 to 11 depending on the species from which the cytochrome *c* was isolated (*2*). For yeast iso-1-cytochrome *c*, site-directed mutagenesis studies have identified lysines 73 and 79 as the heme ligands in the alkaline conformer (*3*, *4*). However, the identity of the ionizable group which triggers the alkaline conformational transition has been widely debated (*4*, *5*). Recent studies on iso-1-cytochrome *c* variants which replace Lys 73 with His have shown that ionization of His 73 triggers population of the His 73−heme alkaline conformer and that two other ionizable groups also affect the kinetics of this conformational change (*6*, *7*).

We have recently been interested in modulating the properties of conformational gates that control electron transfer reactions (*8*). The alkaline conformer of cytochrome *c* is well-known to act as a conformational gate that controls the rate of electron transfer into oxidized cytochrome *c* (*8*−*11*). This conformational gating may have physiological significance for cytochrome *c* function (*4*, *12*, *13*). For the practical purpose of developing and manipulating the properties of conformational gates that can be used for regulating protein electron transfer reactions, the high pH necessary to populate the alkaline conformer of cytochrome *c* is inconvenient. So, cytochrome *c* variants with alkaline states that populate near neutral pH would be useful. Mutation of Phe 82 to smaller side chains has been successful at moving the midpoint of the alkaline conformational transition to near pH 7 (*14*).

Recent thermodynamic analyses of the structural hierarchy of cytochrome *c* suggest that mutations in the least stable N-yellow substructure of cytochrome *c* (Figure 1), comprising an Ω loop that runs from residues 40 to 57 (*15*, *16*), would provide a reasonable strategy to make the alkaline conformer accessible at lower pH. A number of studies (*17*−*21*) show that the alkaline conformational transition involves unfolding of the red substructure, a surface Ω loop running from residues 70−85, of cytochrome *c* (Figure 1). The red substructure is next in stability to the N-yellow substructure (*15*, *16*). We have recently shown that stabilizing mutations at position 52 in the N-yellow substructure of iso-1-cytochrome *c* lead to stabilization of the red substructure as demonstrated by formation of the alkaline conformer at higher pH (*22*). These results are consistent with sequential unfolding of substructures based on relative stability (*23*, *24*).

† This work was supported by NSF Grant CHE 0316378 (to B.E.B.). The Applied Photophysics π*-180 spectrometer was purchased with NIH Grant 1 S10 RR16632-01. The Bruker Daltonics Reflex IV MALDI-TOF mass spectrometer was purchased with NSF Grant CRIF 0234954.

* To whom correspondence should be addressed. Phone: (303) 871-2985. Fax: (303) 871-2254. E-mail: bbowler@du.edu.

10.1021/bi0524971 CCC: $33.50
Published on Web 03/15/2006

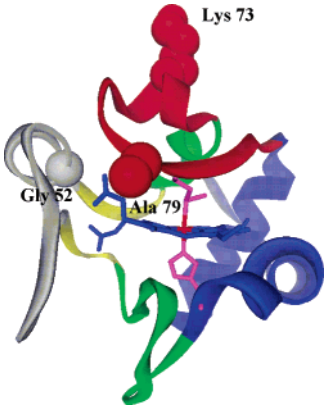

FIGURE 1: Yeast iso-1-cytochrome *c* in the oxidized state, with the Asn 52 → Gly and Lys 79 → Ala mutations of the A79G52 variant, is shown with the substructure classifications of horse cytochrome *c* according to refs *15* and *16*. The substructures are color coded in gray (N-yellow, residues 40−57), red (residues 71−85), yellow (residues 37−39, 58−61), green (60's helix and 20's−30's loop), and blue (N- and C-terminal helices) in order of increasing stability. The heme (blue) and its ligands (magenta), His 18 and Met 80, are shown as stick models. Lys 73, which is the heme ligand in the alkaline conformer, Ala 79, and Gly 52 are shown as space-filling models (α carbon and side chain atoms) in the color of their substructure. The figure was prepared with DS ViewerPro software and the Protein Data Bank file 2YCC (*44*).

Thus, destabilizing mutations at position 52 should also destabilize the red substructure and make formation of the alkaline conformer possible at lower pH. Extensive studies on the effects of mutations at position 52 of iso-1-cytochrome *c* indicate that a glycine at this position is destabilizing (*25*).

Therefore, in the present work, we have introduced the Asn 52 to Gly mutation into wild-type (WT)[1] iso-1-cytochrome *c*. To further simplify the properties of the alkaline conformer, we have prepared the Gly 52 mutation (G52) so that only a single lysine, 73 or 79, is available to bind to the heme in the alkaline conformer by replacing Lys 73 with Ala (A73G52 variant) or Lys 79 with Ala (A79G52 variant; see Figure 1). We find that the alkaline conformational transition is shifted near neutral pH. The Gly 52 mutation also makes the acid transition less cooperative.

MATERIALS AND METHODS

Preparation of Iso-1-cytochrome c Variants. The A73G52 and A79G52 variants were produced by the unique restriction site elimination site-directed mutagenesis method (*26*), as previously described (*27*). Single-stranded pRS/C7.8 DNA (*27*) carrying the Asn 52 → Gly mutation (Grover and Bowler, unpublished results) was used as the template for mutagenesis. All variants contain the mutation Cys 102 → Ser to prevent intermolecular disulfide bond formation during physical studies. Single-stranded DNA was prepared from TG-1 *Escherichia coli* cells with the R408 helper phage (*28*), using phenol extraction methods (*29*) to remove the phage protein coat. The selection oligonucleotide SacI^{-}II^{+} (*27*) was used to eliminate the unique *Sac*I restriction site upstream from the iso-1-cytochrome *c* gene (*CYC1*) and restore the *Sac*II restriction site. The mutagenic oligonucleotides, K73A and K79A [5′-d(CCAGGAATATAAGCCTTTGGGTTAG)-3′ and 5′-d(CAAAGGCCATAGCGGTACCAGG)-3′, respectively; mutation sites underlined], were purchased from Biosynthesis, Inc. (Lewisville, TX). pRS/C7.8 double-stranded DNA (dsDNA) isolated (Promega, Wizard SV+ miniprep kit) from TG-1 *E. coli* cells containing DNA from the mutagenesis reaction was first screened by carrying out *Sac*I and *Sac*II restriction enzyme digests and then sequenced by PCR methods (Quick Start kit; Beckman Coulter, Inc.). The sequencing reactions were then analyzed with a Beckman-Coulter CEQ XLS 8000 capillary electrophoresis autosequencer.

After large-scale preparations of pRS/C7.8 dsDNA (Qiagen MidiPrep kit) carrying the desired mutations, the pRS/C7.8 dsDNA was transformed into the GM-3C-2 cell line (*30*, deficient in cytochrome *c*) of *Saccharomyces cerevisiae* by the LiCl method (*31*). The transformed yeast were characterized by phenotypic screening, a curing procedure to ensure phagemid-based expression, and phagemid recapture followed by DNA sequencing to be certain that no additional mutations were introduced into the *CYC1* gene under the conditions of selective pressure used to express iso-1-cytochrome *c* in *S. cerevisiae*, as described previously (*32*). Protein was isolated and purified from *S. cerevisiae* as previously described (*33*−*35*) with modifications to the final HPLC purification procedure, as described below.

Purification by HPLC cation-exchange chromatography (Waters ProteinPak SP 8 HR column) used a previously described gradient (*35*). After the preceding CM-Sepharose chromatography step (*33*), which is carried out in the presence of β-mercaptoethanol, both variant proteins were ∼80% oxidized. Thus, both proteins were fully oxidized with $K_3Fe(CN)_6$ (4 mg added to a 3 mL solution of ∼6 mg of protein in 50 mM sodium phosphate buffer) prior to HPLC purification, rather than reduced with sodium dithionite, as usual. Since the protein was largely oxidized in the presence of β-mercaptoethanol, air oxidation of the reduced form was expected to be significant during HPLC purification, leading to doubling of the peaks in the chromatogram. Multiple heme-containing peaks were observed in the chromatograms of both variants (see Results) requiring repurification of the major peak to produce a homogeneous product. The concentration of the final product was then measured as described previously (*34*). The protein was then concentrated in Centricon concentrators (Millipore), exchanged into 50 mM sodium phosphate, pH 7, and concentrated to a final volume of ∼500 μL. Mass spectrometry was carried out with a Bruker Daltonics Reflex IV MALDI-TOF mass spectrometer using a matrix containing 10 mg of sinapic acid (Fluka) in 1 mL of 30% acetonitrile containing 0.1% trifluoroacetic acid.

Oxidation of Iso-1-cytochromes c. Even though the A79G52 variant appears to prefer the oxidized state, to ensure that the purified protein was fully oxidized, a few crystals of $K_3Fe(CN)_6$ were added to the protein, and the solution was incubated at 4 °C for 30 min. The solution was then run through a G-25 size exclusion column preequilibrated with the appropriate buffer for the experiment. After the

[1] Abbreviations: WT, wild-type iso-1-cytochrome *c* containing the mutation Cys 102 → Ser; A79G52, variant of WT iso-1-cytochrome *c* carrying Lys 79 → Ala and Asn 52 → Gly mutations; A73G52, variant of WT iso-1-cytochrome *c* carrying Lys 73 → Ala and Asn 52 → Gly mutations; H73, variant of WT iso-1-cytochrome *c* carrying Lys 73 → His mutation; A79H73, variant of WT iso-1-cytochrome *c* carrying Lys 73 → His and Lys 79 → Ala mutations; CD, circular dichroism spectroscopy; GdnHCl, guanidine hydrochloride.

protein was collected, its concentration and degree of oxidation were measured as previously described (*34*).

Guanidine Hydrochloride Denaturation Monitored by Circular Dichroism Spectroscopy. Global stability of the A79G52 variant was determined by guanidine hydrochloride (GdnHCl) denaturation monitored by circular dichroism (CD) spectroscopy using an Applied Photophysics π*-180 spectropolarimeter coupled to a Hamilton Microlab 500 titrator, as described previously (*22*). The experiments were done at 25 °C in 20 mM Tris and 40 mM NaCl (CD buffer) at pH 7.5 with 4 μM protein concentration. A 6 M GdnHCl stock solution was prepared using the same CD buffer, and its concentration was determined using refractive index measurements (*36*). The ellipticity was measured at 222 nm; 250 nm was used as a baseline. The ellipticity observed at 222 nm as a function of GdnHCl concentration was fit to eq 1 (*32*), which assumes a linear free energy relationship and two-state unfolding (*36*, *37*):

$$\theta = \{\theta^\circ_N + [(\theta^\circ_D + m_D[\mathrm{GdnHCl}])\exp\{(m[\mathrm{GdnHCl}] - \Delta G^\circ_u(H_2O))/RT\}]\}/\{1 + \exp\{(m[\mathrm{GdnHCl}] - \Delta G^\circ_u(H_2O))/RT\}\} \quad (1)$$

where θ is the ellipticity of the sample, θ°_N is the ellipticity of native protein, θ°_D is the ellipticity of denatured protein at 0 M GdnHCl, m_D is the denaturant dependence of the denatured state ellipticity, m is the GdnHCl concentration dependence of the free energy of unfolding, ΔG_u, and $\Delta G^\circ_u(H_2O)$ is the free energy of unfolding extrapolated to 0 M GdnHCl. A set of three titrations were done, and the parameters were averaged.

pH Titration Experiments at 695 nm. The alkaline transition of the A79G52 variant was monitored by measuring the absorbance at 695 nm as a function of pH, using previously described methods (*7*). The experiments were done in 500 mM NaCl at 25 °C at 200 μM protein concentration. The titrations were done at 0, 0.3, 0.6, and 0.8 M GdnHCl concentrations.

pH Titration Experiments at the Heme−Soret Band. pH titration experiments were also done at 400 nm, the wavelength of maximum change in absorbance for the conversion between native and the Lys 73-ligated alkaline state. The experiments were done in 500 mM NaCl at 25 °C with about 5 μM final protein concentration in the absence of GdnHCl, over the pH range 4.5−11. Titrations were done as previously described (*7*) except that the absorbance at 400 nm was monitored and the spectrum was scanned from 350 to 700 nm.

pH Jump Experiments with the Stopped-Flow Technique. The experiments were done at 10 μM protein concentration in 500 mM NaCl and at 25 °C. For the upward jumps, the initial pH of the protein was adjusted to pH 6.0 and then jumped from pH 6.0 to a final pH range of 7−10. The buffers used to achieve the final pH were all 20 mM (NaH_2PO_4·H_2O, pH 7.0−7.6; Tris, pH 7.8−8.8; H_3BO_3, pH 9.0−10.0) made in 500 mM NaCl solution. For the downward jumps, the initial pH of the protein solution was adjusted to 8.5 and then jumped to a final range of 6.0−7.0. The buffers used to achieve the final pH were all 20 mM (MES, pH 6.0−6.6; NaH_2PO_4·H_2O, pH 6.8−7.0) made in 500 mM NaCl solution. The experiments were done using the Applied Photophysics π*-180 spectropolarimeter with a stopped-flow unit operating in kinetics mode as described previously (*6*, *7*). The kinetics was monitored with absorption at 400 nm, the wavelength of maximum change in absorbance for the conversion between the native and the alkaline state. Each trial of the upward pH jump data was fit using a single exponential rise to maximum equation:

Scheme 1

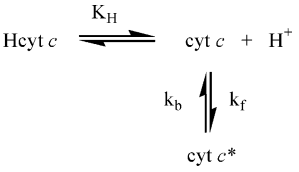

$$A_{400}(t) = A_{400}(0) + a(1 - \exp(-k_{obs}t)) \quad (2)$$

where $A_{400}(t)$ is the absorbance as a function of time at 400 nm, $A_{400}(0)$ is the absorbance at 400 nm at time zero, a is the amplitude, and k_{obs} is the observed rate constant. Each trial of the downward pH jump data was fit using a single exponential decay equation:

$$A_{400}(t) = A_{400}(\infty) + a\exp(-k_{obs}t) \quad (3)$$

where $A_{400}(\infty)$ in the absorbance at 400 nm at infinite time and the other parameters are as defined in eq 2. The rate constants, k_{obs}, for upward and downward pH jumps as a function of pH, extracted from eqs 2 and 3, were fit to the mechanism in Scheme 1 using the equation (*38*):

$$k_{obs} = k_b + k_f K_H/(K_H + [H^+]) \quad (4)$$

where k_{obs} is the observed rate constant, k_f and k_b are the forward and backward rate constants for the alkaline transition, respectively, and K_H is the acid ionization constant for the group which triggers the alkaline transition.

RESULTS

HPLC Purification of the Variants. HPLC purification of the variant A73G52 by cation-exchange chromatography gave four major heme-containing peaks (Figure S1; see Supporting Information). The third peak was the largest and was assumed to be the native form of the A73G52 variant. This peak was repurified across the same column; however, it still produced two overlapping peaks of almost equal intensity (Figure S2). Given the poor prospects of obtaining a homogeneous sample of the A73G52 variant, no further work was carried out with this protein.

HPLC purification of the A79G52 variant by cation-exchange chromatography produced six different peaks (Figure S3). The peak with the highest intensity (peak 5) was inferred to be the native form of the protein, and it was repurified on the same column, producing a homogeneous sample of the A79G52 variant (Figure S4). MALDI-TOF mass spectrometry for this purified material gave a molecular weight of 12577.09, consistent with the expected molecular weight of the A79G52 variant (12580.18). All experiments were done with this material.

Thermodynamic Studies by GdnHCl Denaturation. The global stability of the A79G52 variant was determined using GdnHCl denaturation monitored by CD spectroscopy. The

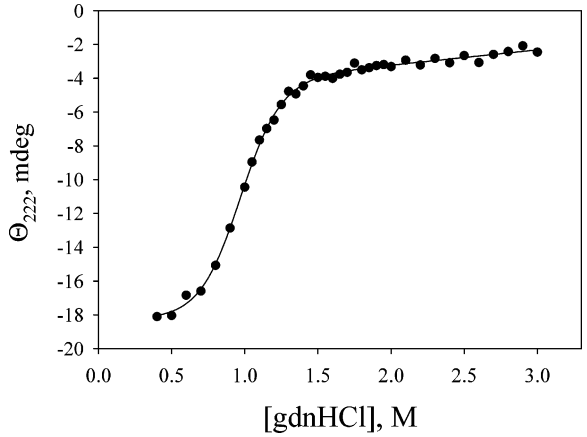

FIGURE 2: Plot of ellipticity at 222 nm versus GdnHCl concentration for the A79G52 variant. GdnHCl denaturation was done in the presence of 20 mM Tris, pH 7.5, and 40 mM NaCl at 25 °C. The curve represents a nonlinear least-squares fit of the data to eq 1 in Materials and Methods.

ellipticity measured at 222 nm plotted against the [GdnHCl] is shown in Figure 2. The thermodynamic parameters obtained from fitting the data to eq 1 (Materials and Methods) are $\Delta G°_u(H_2O) = 4.00 \pm 0.10$ kcal/mol and $m = 4.10 \pm 0.11$ kcal/(mol·M), yielding a denaturation midpoint concentration, $C_m = 0.97$. Thus, both the stability and the *m*-value are decreased significantly relative to WT iso-1-cytochrome *c* [$\Delta G°_u(H_2O) = 5.77 \pm 0.40$ kcal/mol, $m = 5.11 \pm 0.36$ kcal/(mol·M), $C_m = 1.13$; see ref *39*]. The lower *m*-value compared to the WT could be due to greater exposure of buried hydrophobic surface area in the "native" state due to initial partial unfolding of the protein to a Lys 73 alkaline form. The *m*-value is somewhat larger than observed for global unfolding of variants with a His 73 mutation [A79H73 and H73 give $m \sim 3.6$ kcal/(mol·M); see refs *7* and *17*] which unfold from a partially unfolded form with His 73−heme ligation.

Partial Unfolding Monitored at 695 nm by pH Titration Experiments. The absorbance at 695 nm was monitored as a function of pH at various GdnHCl concentrations (Figure 3A). Data for the alkaline transition of the A79H73 variant (*7*) showed that the Lys 79 → Ala mutation causes the alkaline transition to depend on NaCl concentration. This salt dependence saturated at 500 mM NaCl, so all thermodynamic and kinetic alkaline transition data were acquired in the presence of 500 mM NaCl for the A79G52 variant. The data show that the variant exists in the native state (state III) at about pH 6, and as the pH increases, Lys 73 starts replacing the Met 80 bound to the heme (since Lys 79 is absent in this variant, only Lys 73 remains as a ligand to replace Met 80 during the alkaline transition; see refs *3* and *4*) near pH 7 and becomes the sole ligand at higher pH. As the GdnHCl concentration increases, the protein no longer becomes fully native between the acid and alkaline states. We note that, in the presence of [GdnHCl], precipitation problems were encountered below pH 4, so data were not collected below this pH. Similar problems were encountered for an A79H73 variant (*7*). A fit of the data from pH 6 to pH 9 (0 M GdnHCl) in Figure 3A to the Henderson−Hasselbalch equation, assuming a 1 proton process, yields an apparent pK_a of 7.46 ± 0.02 for the alkaline transition.

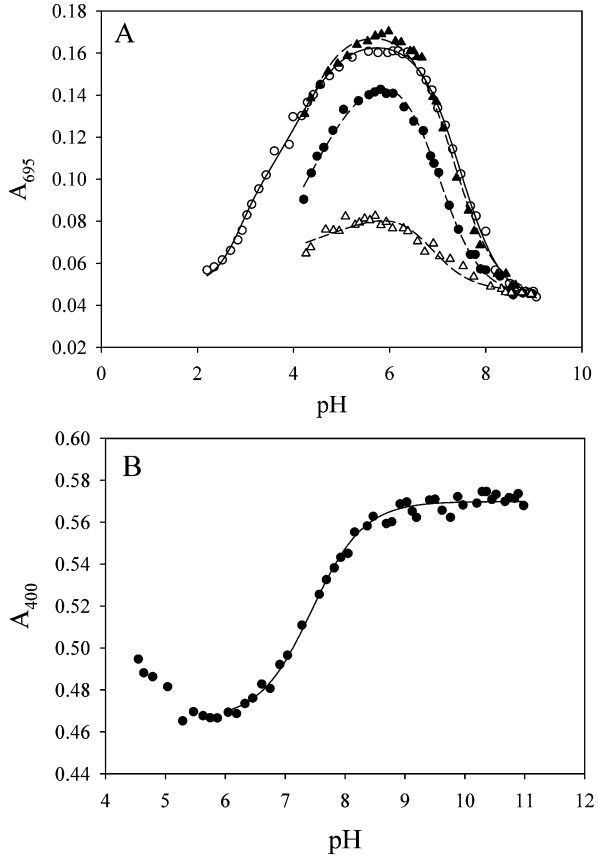

FIGURE 3: (A) Plots of absorbance data at 695 nm in 0 M (○), 0.3 M (▲), 0.6 M (●), and 0.8 M (△) GdnHCl versus pH for the A79G52 variant in 0.5 M NaCl at 25 °C. The curve for the 0 M GdnHCl (solid line) is a fit to eq 8 in the Discussion. The curves (dashed lines) for the 0.3, 0.6, and 0.8 M GdnHCl data are fits to eq 9 in the Discussion. (B) Plot of absorbance at 400 nm versus pH for the A79G52 variant done with 5 μM protein in 500 mM NaCl and no GdnHCl at 25 °C. The solid curve is a fit of the data from pH 6.0 to pH 11.0 to the Henderson−Hasselbalch equation.

Partial Unfolding Monitored at 400 nm by pH Titration Experiments. pH titration experiments done at 400 nm and 5 μM final protein concentration (Figure 3B) produced data similar to that at 695 nm (Figure 3A), indicating that the two absorbance bands monitor the same process. The variant exists in the native form at about pH 6, as indicated by data from both 695 and 400 nm bands; then at higher pH values Met 80 is replaced by Lys 73. The data from pH 6.0 to pH 11.0 were fit to the Henderson−Hasselbalch equation, yielding an apparent pK_a of 7.44 ± 0.03 for the alkaline transition of the G52A79 variant.

The Alkaline Transition Monitored Using pH Jump Stopped-Flow Methods. Thermodynamic data for the A79G52 variant (Figure 3) indicate that Lys 73 starts replacing Met 80 at about pH 7.0. For upward pH jumps, the initial pH of the protein was set to 6.0, where equilibrium data indicate that the A79G52 variant is completely native (Figure 3). Data were collected at final pH values from 7.0 to 10.0. For downward pH jumps, the initial pH was 8.5, since equilibrium data (Figure 3) indicate that the A79G52 variant is essentially completely alkaline at this pH. Data were collected for final pH values from 6 to 7. Data were not collected below pH 6 because of the onset of acid denaturation (Figure 3). All data were collected in the presence of 500 mM NaCl

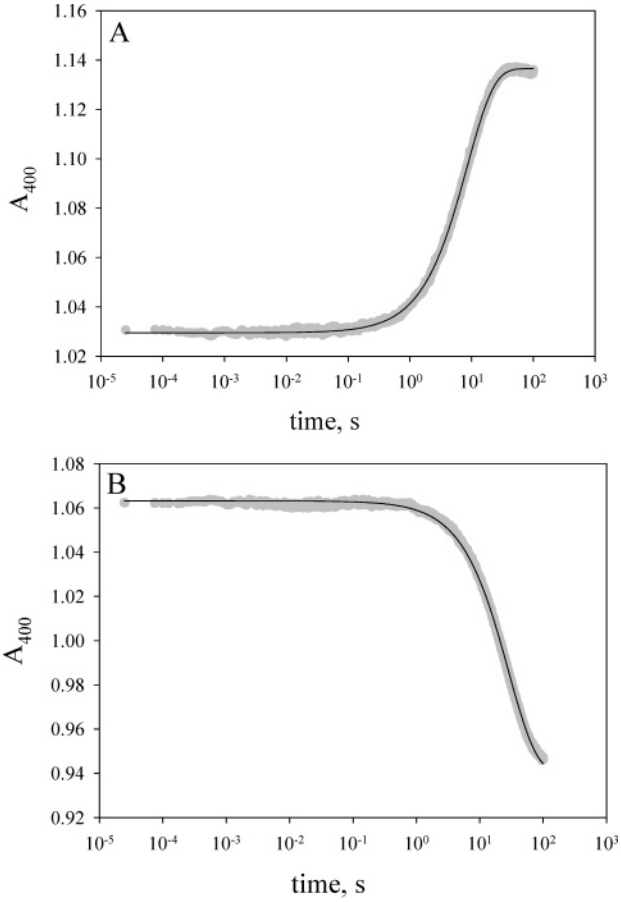

FIGURE 4: Plot of A_{400} versus time (logarithmic scale) for the A79G52 iso-1-cytochrome *c* variant from pH jump stopped-flow measurements. (A) Upward jump from pH 6 to pH 8 in 0.5 M NaCl at 25 °C with the protein concentration around 10 μM. The gray dots are the data at 400 nm, and the solid black curve is the fit of the data to a single exponential rise to maximum equation (eq 2 in Materials and Methods). (B) Downward jump from pH 8.5 to pH 6 in 0.5 M NaCl at 25 °C with the protein concentration around 10 μM. The gray dots are the data at 400 nm, and the solid black curve is the fit of the data to a single exponential decay equation (eq 3 in Materials and Methods).

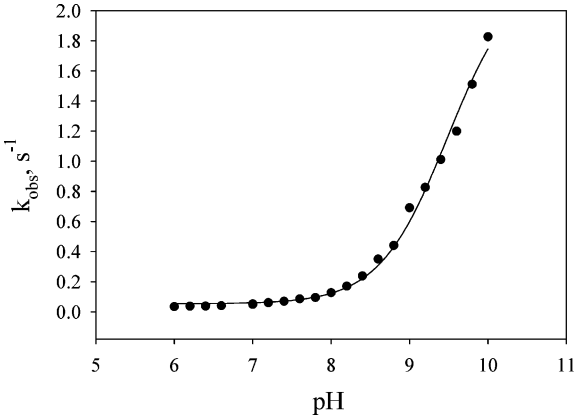

FIGURE 5: Plot of k_{obs} versus pH for the A79G52 variant for both upward and downward pH jump data in 0.5 M NaCl at 25 °C with the protein concentration around 10 μM. The curve is a fit of the data to eq 4 (Materials and Methods). Parameters from the fit are given in the text.

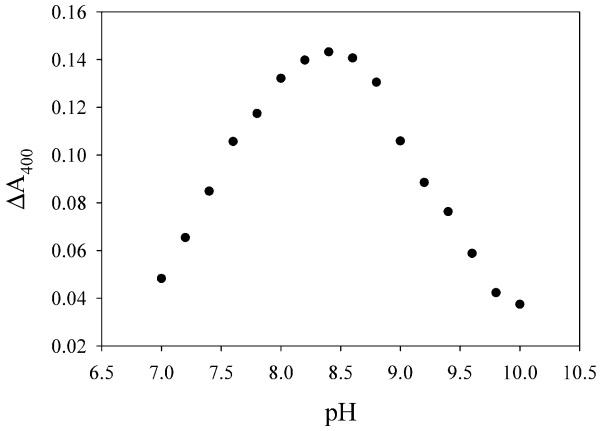

FIGURE 6: Plot of change in amplitude, ΔA_{400}, versus pH for upward pH jump data for the alkaline transition of the A79G52 variant. Data were collected in 0.5 M NaCl at 25 °C with protein concentration around 10 μM. The amplitude data from pH 8.4 to pH 10.0 when fit to the Henderson−Hasselbalch equation yield an apparent pK_a of 9.20 ± 0.08.

for the reasons described above. Typical data for upward and downward pH jumps are shown in Figure 4. The data are consistent with a single kinetic phase with rate constants between 0.03 and 1.8 s^{-1} (Tables S1 and S3). Figure 5 shows the pH dependence of the observed rate constant, k_{obs}, for both upward and downward pH jump data. The k_{obs} remains constant from about pH 6 to pH 7, then slowly starts increasing from pH 7.0 to pH 8.0, and then increases faster from pH 8.0 to pH 10.0. The k_{obs} versus pH data were fit to eq 4 in Materials and Methods yielding $k_b = 0.05 \pm 0.01$ s^{-1}, $k_f = 2.21 \pm 0.08$ s^{-1}, and p$K_H = 9.48 \pm 0.04$. The conformational equilibrium constant, K_C, for the alkaline transition determined from k_f/k_b is 44 ± 9, which is within a factor of 2 of the value determined thermodynamically (117 ± 8; see Discussion). Fitting the k_{obs} versus pH data to a linearized form of eq 4 (*14*) gave p$K_H \sim 9.2$ and $k_f/k_b \sim 42$.

The amplitude data for the alkaline transition for the upward jumps are shown in Figure 6 (see also Table S2). The amplitude increases from pH 7.0 to pH 8.5 and then decreases at higher pH values. The increase in the amplitude is consistent with Lys 73 replacing the Met 80 heme ligand. The amplitude data from pH 8.4 to pH 10.0 when fit to the Henderson−Hasselbalch equation gave an apparent pK_a value of ∼9.2, similar to the pK_H obtained from the plot of k_{obs} versus pH (Figure 5). A faster process ($k_{obs} \sim 40-50$ s^{-1}; see Table S5) is observable above pH 9, but it is low amplitude. Thus, the loss in amplitude is likely primarily due to a fast process that is within the dead time of our stopped-flow experiments.

DISCUSSION

Global Stability of the A79G52 Variant at pH 7.5. The *m*-value for unfolding of the A79G52 variant at pH 7.5 is much lower than observed for the WT protein [∼4.1 versus ∼5.1 kcal/(mol·M)]. This behavior is reminiscent of variants containing mutations of Lys 73 to His (*7*, *17*−*19*), although the *m*-value is somewhat larger for the A79G52 variant. The similarity in behavior is not surprising since the A79G52 variant and the His 73 variants (H73 and A79H73) are all partially unfolded by a heme−ligand exchange reaction involving a ligand at sequence position 73. The GdnHCl unfolding midpoint for the His 73 variants is higher ($C_m \sim$ 1.15 M), and the onset of CD-monitored unfolding is somewhat higher (∼0.8−0.9 M), where partial unfolding to

Scheme 2

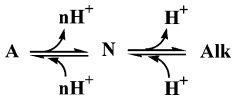

the His 73 alkaline conformer is nearly complete (*7*, *19*). Due to the lower C_m for the A79G52 variant, the onset of CD-monitored unfolding at pH 7.5 is 0.5−0.6 M GdnHCl (Figure 2). From Figure 3, it is evident that partial unfolding is only about two-thirds complete at this GdnHCl concentration at pH 7.5. Thus, the somewhat higher *m*-value for global unfolding for the A79G52 variant relative to the His 73 variants may reflect the lesser degree of partial unfolding at the onset of CD-monitored GdnHCl denaturation. However, as with the His 73 variants, the decreased stability and *m*-value of the A79G52 variant relative to the WT protein are attributable to "global" unfolding proceeding from a partially unfolded state of the protein.

The population of partially unfolded "alkaline" conformers during denaturant unfolding of iso-1-cytochrome *c* is clearly enhanced in the A79G52 variant and His 73 variants of iso-1-cytochrome *c* relative to the WT protein. However, NMR studies of horse ferricytochrome *c* at pH 7 also demonstrate the population of these intermediates during denaturant unfolding (*40*, *41*). Thus, even when not specifically stabilized, alkaline conformers of cytochrome *c* appear to be important equilibrium unfolding intermediates for this protein. It is also interesting to note that the CD-monitored stabilities of the H73, A79H73, and A79G52 variants are all similar, suggesting that neither the Ala 79 mutation nor the Gly 52 mutation significantly affects CD-monitored global stability. This observation is consistent with hydrogen exchange (*21*) and NMR (*42*) data which suggest that both the red (residues 70−85) and N-yellow (residues 40−57) substructures (*16*) are disrupted in the alkaline state of cytochrome *c* (see Figure 1).

Acid Transition of the A79G52 Variant. The pH dependence of the 695 nm absorption in 500 mM NaCl at 0 M GdnHCl (Figure 2) shows that the A79G52 variant exists in the native state at pH 6.0. The acid transition occurs from pH 6.0 to pH 2.0 and the alkaline transition from pH 6.0 to pH 9.0 (Lys 73 replacing Met 80 ligated to the heme). Attempts to fit the data to the simple three-state equilibrium (Scheme 2) used in our work on the A79H73 variant (*7*) proved unsuccessful.

Closer scrutiny of the spectra between 570 and 750 nm demonstrated that the acid transition between pH 2 and pH 6 can be broken up into two processes with distinct isosbestic points (Figures S5 and S6). Over the pH range 2−4 the isosbestic point is at 596 nm, and for the pH range 4−6 it is at 644 nm, indicating that the acid transition is a three-state process. The absorbance values at these two wavelengths were plotted as a function of pH and were separately fit to an "*n*" proton, two-state process using the equation:

$$A = (A' + A''K_{obs})/(1 + K_{obs}) \qquad (5)$$

where A is the absorbance at either 596 or 644 nm, A' is the absorbance of the low pH state, A'' is the absorbance of the high pH state, and K_{obs} has the form given in the equation:

$$K_{obs} = \frac{K_C}{1 + ([H^+]/K_a)^n} = \frac{10^{-pK_c}}{1 + 10^{n(pK_a - pH)}} \qquad (6)$$

In eq 6, K_C is the conformational equilibrium constant, n is the number of protons involved in the transition, and K_a is the ionization constant of the group(s) responsible for the conformational transition. The fits of the acid transition (pH 2−6) data at 596 and 644 nm to eq 5 are shown in Figure 7. The parameters obtained from these fits are given in the Table 1. The data indicate that there are two separate processes, one at low pH involving ∼1.7 protons and the other at higher pH involving ∼1.3 protons.

On the basis of the results from the plots at 596 and 644 nm, the three-state equilibrium mechanism shown in Scheme 3 is consistent with the properties of the acid transition of the A79G52 variant. In Scheme 3, A_1 is the low pH acid state which is in equilibrium with the higher pH acid state, A_2, which in turn is in equilibrium with the native state, N,

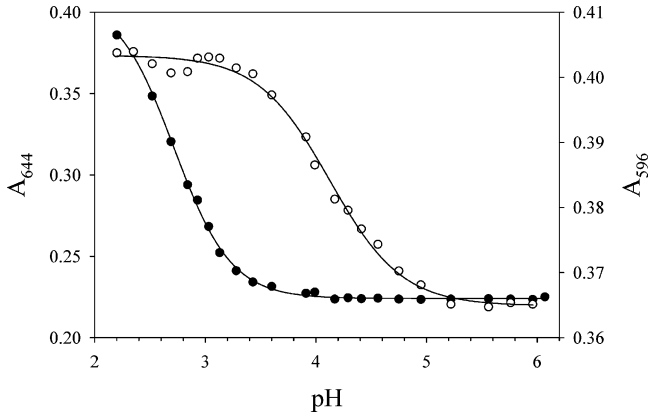

FIGURE 7: Acid transition monitored at isosbestic points, 596 nm (○) and 644 nm (●). The low pH isosbestic point (596 nm) monitors the higher pH phase ($A_2 \rightarrow N$), and the high pH isosbestic point (644) monitors the lower pH phase ($A_1 \rightarrow A_2$) of the acid transition. For data at 596 nm, the pK_a in eq 6 was set to 6, and for the data at 644 nm, it was set to 4. Experimental conditions are as for the 0 M GdnHCl data in Figure 3.

Table 1: Thermodynamic Parameters for the Acid Transition of the A79G52 Variant in 500 mM NaCl and at 25 °C from Fits of Data at Different Wavelengths

	low pH phase[a]		high pH phase[b]	
wavelength, nm	pK_{C1}	n_1	pK_{C2}	n_2
596[c]			-2.5 ± 0.2	1.3 ± 0.1
644[c]	-2.15 ± 0.05	1.7 ± 0.1		
570	-1.9 ± 0.3	1.7 ± 0.2	-1.5 ± 0.2	0.8 ± 0.2
630	-1.7 ± 0.5	1.4 ± 0.4	-1.9 ± 0.2	1.0 ± 0.2
695	-1.5 ± 0.6	1.6 ± 0.4	-2.0 ± 0.3	1.1 ± 0.3

[a] The pK_a value for the ionizable groups involved in the low pH phase of fits using eq 5 or 7 was taken as 4 assuming ionization of the carboxylate group of an Asp or Glu. Therefore, the magnitude of pK_{C1} is not absolute. [b] The pK_a value for the ionizable groups involved in the high pH phase of fits using eq 5 or 7 was taken as 6 assuming ionization of the imidazole group of a His or the carboxylate of a heme propionate. Therefore, the magnitude of pK_{C2} is not absolute. [c] Only one phase is observed since these are isosbestic points.

Scheme 3

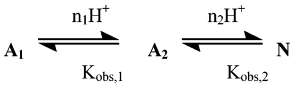

Scheme 4

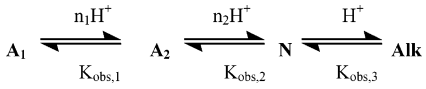

with equilibrium constants, $K_{obs,1}$ and $K_{obs,2}$, respectively. From this mechanism, eq 7 can be derived:

$$A = A_N + \frac{(A_{A1} - A_N) + K_{obs,1}(A_{A2} - A_N)}{1 + K_{obs,1}(1 + K_{obs,2})} \quad (7)$$

where A is the absorbance at the wavelength monitored, A_N is the absorbance of the native state, A_{A1} is the absorbance of the low pH acid state, A_{A2} is the absorbance of the higher pH acid state, and $K_{obs,1}$ and $K_{obs,2}$ are the observed equilibrium constants for the transitions, $A_1 \rightarrow A_2$ and $A_2 \rightarrow N$, respectively, and have the same form as eq 6.

This mechanism was used to fit the acid transition data (pH 2−6) at 695 nm in the absence of GdnHCl (Figure 3) as well as data at two other wavelengths (570 and 630 nm) where there is maximal change in the absorbance values during the acid transition (see Figures S7 and S8). The parameters obtained by fitting the absorbance data at these wavelengths to eq 7 are given in Table 1. From the above data, it can be seen that the low pH (2−4) transition involves ~1.6 protons and the higher pH (4−6) transition ~1.0 proton. The midpoint pH values for these transitions obtained from eq 6 with the parameters in Table 1 are ~2.9 and ~4.1. The midpoint pH values and the number of protons involved in each phase are similar to data for the acid transition of the A79H73 variant (*7*). We attributed the loss of cooperativity for the acid transition of the A79H73 variant to perturbation of the buried hydrogen bond network of iso-1-cytochrome *c* in which Lys 79 participates and the concomitant effect on the long-range His 26/Glu 44 hydrogen bond. However, the details of the loss of cooperativity are different. For the A79H73 variant, the heme stays low spin in the high pH phase of the acid transition, and Met 80 ligation is completely lost (loss of absorbance at 695 nm). In the case of the A79G52 variant, loss of Met 80 ligation is spread out over both phases of the acid transition as is formation of a high-spin state (growth in absorbance at 630 nm). Presumably the latter difference is caused by the Gly 52 mutation although the Lys 73 → His mutation in the A79H73 variant may have an effect as well. The structural details of the effect of the Gly 52 mutation on the acid transition are unclear at this point.

Alkaline Transition of the A79G52 Variant. An important goal of this work was to make the alkaline state of iso-1-cytochrome *c* more accessible by destabilizing the N-yellow substructure (see Figure 1). Fits of data at either 695 or 400 nm show that the apparent pK_a for this transition has dropped to ~7.45, about 1.2 units lower than for the WT protein (*4*, *17*) and about 1 unit lower than for a Lys 79 → Ala (A79) variant (*4*). The decrease in the apparent pK_a is comparable to the effects of mutations at position 82 in the red substructure (*14*).

From the previous section, it is clear that the acid transition in the A79G52 variant is not monophasic but is a three-state process. To fit the entire data set in Figure 2A from pH 2 to pH 9 (at 0 M GdnHCl in 500 mM NaCl), a four-state process which includes both acid and alkaline transitions is necessary, as outlined in Scheme 4. In Scheme 4, Alk is the alkaline state and $K_{obs,3}$ is the observed equilibrium constant for the alkaline transition and has the form given in eq 6 with $n = 1$.

Table 2: Thermodynamic Parameters from Fits of the Acid and Alkaline Transition Data of the A79G52 Variant in 500 mM NaCl and at 25 °C as a Function of GdnHCl Concentration

[GdnHCl], M	pK_{C2} for acid transition	no. of protons in acid transition	pK_{C3} for alkaline transition
0[a]			−2.07 ± 0.03
0.3[b]	−1.95 ± 0.19	0.93 ± 0.11	−2.17 ± 0.04
0.6[b]	−0.98 ± 0.03	0.62 ± 0.02	−2.53 ± 0.02
0.8[b]	0.09 ± 0.03	0.26 ± 0.08	−3.18 ± 0.08

[a] The pK_{C3} parameter is from a fit of the data to eq 8. [b] Parameters are from a fit of the data to eq 9.

The absorbance data at 695 nm at 0 M GdnHCl (Figure 2A) can now be fit to the equation:

$$A = A_{alk} + \frac{(A_{A1} - A_{alk}) + K_{obs,1}[(A_{A2} - A_{alk}) + K_{obs,2}(A_N - A_{alk})]}{1 + K_{obs,1}[1 + K_{obs,2}(1 + K_{obs,3})]} \quad (8)$$

which is derived from Scheme 4, where A_{alk} is the absorbance at 695 nm of the alkaline state and the other parameters are as in eq 7. The curve obtained by fitting the data at 0 M GdnHCl to this equation is shown in Figure 3A. In fitting the data, pK_{a1} and pK_{a2} were taken as 4 (assuming a carboxylate side chain) and 6 (assuming a histidine or heme propionate), respectively, and the value of pK_{a3} was set to 9.5, the value of this parameter from the pH jump kinetic data for the alkaline transition. The parameters for the acid transition are within error of the values obtained from fitting the acid transition separately, although the errors are larger, in large part due to the uncertainty in A_{A2}. The pK_{C3} for the alkaline transition was also obtained by fitting the data from pH 6 to pH 9 to eq 5 with the pK_a of the ionizable trigger group set to 9.5. The value of pK_{C3} obtained from this fit was −2.03 ± 0.02, within error of the value obtained for the alkaline transition by fitting the data in Figure 3A to eq 8 (Table 2).

The data at 0.3, 0.6, and 0.8 M GdnHCl were fit to a three-state equilibrium (Scheme 2, eq 9), because low pH data could not be recorded in the presence of GdnHCl due to precipitation problems:

$$A = A_{alk} + \frac{(A_A - A_{alk}) + K_{obs,3}(A_N - A_{alk})}{1 + K_{obs,2}(1 + K_{obs,3})} \quad (9)$$

In these fits, $K_{obs,2}$ and $K_{obs,3}$ have the form of eq 6, pK_{a2} was assumed to be 6, and the pK_{a3} value for the alkaline transition was set to 9.5, as described above. Since A_A was not available from the data, it was assumed to be equal to A_{alk}. For data where the fully native state was not achieved near pH 6, $(A_N - A_{alk})$ was set to the value obtained at 0 M GdnHCl. The fits for the data at 0.3, 0.6, and 0.8 M GdnHCl are shown in the Figure 3. The parameters obtained from these fits are given in Table 2.

Fits to the data at 0.3, 0.6, and 0.8 M GdnHCl were also attempted where the parameter for the number of protons involved in the acid transition was fixed to 0.9, as observed at 0.3 M GdnHCl (and similar to the value for the A_2 to N

transition at 0 M GdnHCl). However, much poorer fits to the data were obtained. So the parameter n in eq 9 was allowed to float. As the GdnHCl concentration increased, n was observed to decrease (Table 2). The decrease may not be realistic and may contribute to uncertainty in the parameters obtained from these data fits.

The pK_C values for the alkaline transition as a function of [GdnHCl] were converted to free energies using $\Delta G = 2.3 RT\text{p}K_C$ and fit to a linear free energy relationship giving an m-value of 1.8 ± 0.5 kcal/(mol·M) and $\Delta G_u(H_2O)$ for formation of the alkaline state in the limit of high pH of −2.6 ± 0.3 kcal/mol. The m-value is consistent with the m-values obtained for formation of the His 73 iso-1-cytochrome *c* alkaline state (*17*, *19*, *22*). So, it appears that from a thermodynamic standpoint the degree of unfolding in the alkaline state of this variant is similar to previously characterized alkaline states involving ligation from ligands at position 73.

Kinetics of Formation of the Alkaline State of the A79G52 Variant. The pH jump experiments done on the A79G52 variant indicate one kinetic phase up to pH ∼9.0. A fit of k_{obs} versus pH data to eq 4 (Figure 5) yields k_b ∼0.05 s^{-1}, which is within error of the value reported previously for an A79 variant (*4*) which also has Lys 73 heme ligation in the alkaline state. k_{obs} grows considerably faster for the A79G52 variant than for the A79 variant above pH 8, yielding k_f and pK_H considerably smaller than for the A79 variant (k_f of ∼2.2 versus ∼160 s^{-1} and pK_H of ∼9.5 versus 12; see ref *4*). The kinetic data for the A79 variant were collected at 100 mM NaCl rather than the 500 mM NaCl used here. Equilibrium data on the alkaline transition of the A79 variant show a salt dependence (*4*). However, this salt dependence would only account for a factor of ∼2 in k_f. Thus, the Gly 52 mutation appears to be primarily responsible for the differences in the kinetics of the alkaline conformational transition.

pK_H values for the alkaline conformational transition between 9.0 and 9.5 have previously been observed when Phe 82 is mutated to Leu, Ile, Gly, and Ser (*14*). Interestingly, the amplitude for the Lys 73 ligation kinetic phase decreases with an apparent pK_a of ∼9.2 (Figure 6), similar to the pK_H for the growth of k_{obs}. The absorbance values in the Soret band pH titrations (Figure 3B) increase to pH ∼8.5 and then level off, suggesting that an unstable intermediate forms in advance of Lys 73−heme ligation causing apparent loss in amplitude of the Lys 73−heme binding phase. This transient intermediate also appears to facilitate Lys 73−heme binding since k_{obs} for Lys 73−heme binding increases as this intermediate populates. In our kinetic studies on the H73 (*6*) and the A79H73 (*7*) variants, we observed three ionizations with pK_a's near 5.5, 6.5 (due to His 73), and 9 which affect the kinetics of formation of the His 73−heme alkaline conformer. The pK_H of 9.0−9.5 observed here and for the variants at position 82 (*14*) coincides with the high pH ionization which affects the kinetics of formation of the His 73−heme alkaline conformer. Thus, an ionization near pH 9 appears to affect the kinetics of formation of the alkaline state irrespective of whether the incoming ligand is histidine or lysine. However, for lysine ligation this ionization is difficult to observe if the alkaline conformer is not significantly populated near physiological pH. So, what is the nature of this transient intermediate that enhances the rate of formation of alkaline cytochrome *c* with a pK_a near 9? Our results on the alkaline form of the A79H73 variant (*7*) suggest that this intermediate is high spin, in accord with observations for a Trp 82 → Phe iso-1-cytochrome *c* variant (*43*). As previously suggested (*7*, *43*), this high-spin intermediate could be due to ionization and binding of Tyr 67 to the heme, although other scenarios are possible (*43*).

CONCLUSIONS

The destabilizing Asn 52 to Gly mutation in the least stable substructure of cytochrome *c* allows population of the alkaline state near physiological pH. This effect on the stability of the alkaline state demonstrates that the substructure hierarchy of cytochrome *c* (*15*, *16*) is a useful predictive tool for manipulating the conformational properties of this protein. The shift in the pK_H for the ionizable group which triggers the alkaline conformational transition of the A79G52 variant to ∼9.5 provides additional evidence that an ionizable group with a pK_a between 9 and 9.5 modulates this conformational transition. The combination of the Gly 52 and Ala 79 mutations splits the acid transition into two distinct phases. Since the mutations at both positions 52 and 79 are expected to impact the buried hydrogen bond network of cytochrome *c*, this result suggests that the buried hydrogen bond network of this protein is a key modulator of the acid transition.

SUPPORTING INFORMATION AVAILABLE

Figures S1−S4 showing HPLC data for the A73G52 and A79G52 variants, Figures S5 and S6 showing visible spectra as a function of pH for the A79G52 variant, Figures S7 and S8 showing plots of absorbance as a function of pH at 570 and 630 nm for the A79G52 variant fitted to eq 7, and Tables S1−S5 summarizing rate constants and amplitudes for the alkaline conformational transition of the A79G52 variant. This material is available free of charge via the Internet at http://pubs.acs.org.

REFERENCES

1. Theorell, H., and Åkesson, A. (1941) Studies on cytochrome *c*, *J. Am. Chem. Soc. 63*, 1804−1820.
2. Moore, G. R., and Pettigrew, G. W. (1990) *Cytochromes c: Evolutionary, Structural and Physicochemical Aspects*, pp 184−196, Springer-Verlag, New York.
3. Ferrer, J. C., Guillemette, T. G., Bogumil, R., Inglis, S. C., Smith, M., and Mauk, A. G. (1993) Identification of Lys79 as an iron ligand in one form of alkaline yeast iso-1-ferricytochrome *c*, *J. Am. Chem. Soc. 115*, 7507−7508.
4. Rosell, F. I., Ferrer, J. C., and Mauk, A. G. (1998) Proton-linked protein conformational switching: Definition of the alkaline conformational transition of yeast iso-1-ferricytochrome *c*, *J. Am. Chem. Soc. 120*, 11234−11245.
5. Wilson, M. T., and Greenwood, C. (1996) The alkaline transition in ferricytochrome *c*, in *Cytochrome c: A Multidisciplinary Approach* (Scott, R. A., and Mauk, A. G., Eds.) pp 611−634, University Science Books, Sausalito, CA.
6. Martinez, R. E., and Bowler, B. E. (2004) Proton-mediated dynamics of the alkaline conformational transition of yeast iso-1-cytochrome *c*, *J. Am. Chem. Soc. 126*, 6751−6758.
7. Baddam, S., and Bowler, B. E. (2005) Thermodynamics and kinetics of formation of the alkaline state of a Lys 73→Ala/Lys 73→His variant of iso-1-cytochrome *c*, *Biochemistry 44*, 14956−15968.
8. Baddam, S., and Bowler, B. E. (2005) Conformationally gated electron transfer in iso-1-cytochrome *c*: Engineering the rate of a conformational switch, *J. Am. Chem. Soc. 127*, 9702−9703.

9. Greenwood, C., and Palmer, G. (1965) Evidence for the existence of two functionally distinct forms of cytochrome *c* monomer at alkaline pH, *J. Biol. Chem. 240*, 3660−3663.
10. Wilson, M. T., and Greenwood, C. (1971) Studies on ferricytochrome *c*. 2. A correlation between reducibility and the possession of the 695 nm absorption band of ferricytochrome *c*, *Eur. J. Biochem. 22*, 11−18.
11. Hodges, H. L., Holwerda, R. A., and Gray, H. B. (1974) Kinetic studies of the reduction of ferricytochrome *c* by $Fe(EDTA)^{2-}$, *J. Am. Chem. Soc. 96*, 3132−3137.
12. Döpner, S., Hildebrant, P., Rosell, F. I., and Mauk, A. G. (1998) Alkaline conformational transition of ferricytochrome *c* studied by resonance Raman spectroscopy, *J. Am. Chem. Soc. 120*, 11246−11255.
13. Döpner, S., Hildebrant, P., Rosell, F. I., Mauk, A. G., von Walter, M., Buse, G., and Soulimane, T. (1999) The structural and functional role of lysine residues in the binding domain of cytochrome *c* in the electron transfer to cytochrome *c* oxidase, *Eur. J. Biochem. 261*, 379−391.
14. Pearce, L. L., Gärtner, A. L., Smith, M., and Mauk, A. G. (1989) Mutation-induced perturbation of the cytochrome *c* alkaline transition, *Biochemistry 28*, 3152−3156.
15. Bai, Y., Sosnick, T. R., Mayne, L., and Englander, S. W. (1995) Protein folding intermediates: Native-state hydrogen exchange, *Science 269*, 192−197.
16. Krishna, M. M. G., Lin, Y., Rumbley, J. N., and Englander, S. W. (2003) Cooperative omega loops in cytochrome *c*: Role in folding and function, *J. Mol. Biol. 331*, 29−36.
17. Godbole, S., Dong, A., Garbin, K., and Bowler, B. E. (1997) A lysine 73 → histidine variant of yeast iso-1-cytochrome *c*: Evidence for a native-like intermediate in the unfolding pathway and implications for *m* value effects, *Biochemistry 36*, 119−126.
18. Godbole, S., and Bowler, B. E. (1999) Effect of pH on formation of a nativelike intermediate on the unfolding pathway of a Lys 73 → His variant of yeast iso-1-cytochrome *c*, *Biochemistry 38*, 487−495.
19. Nelson, C. J., and Bowler, B. E. (2000) pH dependence of formation of a partially unfolded state of a Lys 73 → His variant of iso-1-cytochrome *c*: Implications for the alkaline conformational transition of cytochrome *c*, *Biochemistry 39*, 13584−13594.
20. Nelson, C. J., LaConte, M. J., and Bowler, B. E. (2001) Direct detection of heat and cold denaturation for partial unfolding of a protein, *J. Am. Chem. Soc. 123*, 7453−7454.
21. Hoang, L., Maity, H., Krishna, M. M. G., Lin, Y., and Englander, S. W. (2003) Folding units govern the cytochrome *c* alkaline transition, *J. Mol. Biol. 331*, 37−43.
22. Kristinsson, R., and Bowler, B. E. (2005) Communication of stabilizing energy between substructures of a protein, *Biochemistry 44*, 2349−2359.
23. Xu, Y., Mayne, L., and Englander, S. W. (1998) Evidence for an unfolding and refolding pathway in cytochrome *c*, *Nat. Struct. Biol. 5*, 774−778.
24. Goedken, E. R., and Marqusee, S. (2001) Native-state energetics of a thermostabilized variant of ribonuclease HI, *J. Mol. Biol. 314*, 863−871.
25. Hickey, D. R., Berghuis, A. M., Lafond, G., Jaeger, J. A., Cardillo, T. S., McLendon, D., Das, G., Sherman, F., Brayer, G. D., and McLendon, G. (1991) Enhanced thermodynamic stabilities of yeast iso-1-cytochromes *c* with amino acid replacements at positions 52 and 102, *J. Biol. Chem. 266*, 11686−11694.
26. Deng, W. P. D., and Nickoloff, J. A. (1992) Site-directed mutagenesis of virtually any plasmid by eliminating a unique site, *Anal. Biochem. 200*, 81−88.
27. Smith, C. R., Mateljevic, N., and Bowler, B. E. (2002) Effects of topology and excluded volume on protein denatured state conformational properties, *Biochemistry 41*, 10173−10181.
28. Russel, M., Kidd, S., and Kelley, M. R. (1986) An improved filamentous helper phage for generating single-stranded plasmid DNA, *Gene 45*, 333−338.
29. Sambrook, J., and Russell, D. W. (2001) *Molecular Cloning: A Laboratory Manual*, pp 3.26−3.29, Cold Spring Harbor Laboratory Press, Cold Spring Harbor, NY.
30. Faye, G., Leung, D. W., Tatchell, K., Hall, B. D., and Smith, M. (1981) Deletion mapping of sequences essential for the *in vivo* transcription of the iso-1-cytochrome *c* gene, *Proc. Natl. Acad. Sci. U.S.A. 78*, 2258−2262.
31. Ito, H., Fukada, Y., Murata, K., and Kimura, A. (1983) Transformation of intact yeast cells treated with alkali cations, *J. Bacteriol. 153*, 163−168.
32. Hammack, B. N., Smith, C. R., and Bowler, B. E. (2001) Denatured state thermodynamics: Residual structure, chain stiffness and scaling factors, *J. Mol. Biol. 311*, 1091−1104.
33. Redzic, J. S., and Bowler, B. E. (2005) Role of hydrogen bond networks and dynamics in positive and negative cooperative stabilization of a protein, *Biochemistry 44*, 2900−2908.
34. Bowler, B. E., May, K., Zaragoza, T., York, P., Dong, A., and Caughey, W. S. (1993) Destabilizing effects of replacing a surface lysine of cytochrome *c* with aromatic amino acids: Implications for the denatured state, *Biochemistry 32*, 183−190.
35. Bowler, B. E., Dong, A., and Caughey, W. S. (1994) Characterization of the guanidine hydrochloride-denatured state of iso-1-cytochrome *c* by infrared spectroscopy, *Biochemistry 33*, 2402−2408.
36. Pace, C. N. (1986) Determination and analysis of urea and guanidine hydrochloride denaturation curves, *Methods Enzymol. 26*, 266−280.
37. Schellman, J. A. (1978) Solvent denaturation, *Biopolymers 17*, 1305−1322.
38. Davis, L. A., Schejter, A., and Hess, G. P. (1974) Alkaline isomerization of oxidized cytochrome *c*: Equilibrium and kinetic measurements, *J. Biol. Chem. 249*, 2624−2632.
39. Godbole, S., Hammack, B., and Bowler, B. E. (2000) Measuring denatured state energetics: Deviations from random coil behavior and implications for the folding of iso-1-cytochrome *c*, *J. Mol. Biol. 296*, 217−228.
40. Russell, B. S., Melenkivitz, R., and Bren, K. L. (2000) NMR investigation of ferricytochrome *c* unfolding: Detection of an equilibrium unfolding intermediate and residual structure in the denatured state, *Proc. Natl. Acad. Sci. U.S.A. 97*, 8312−8317.
41. Russel, B. S., and Bren, K. L. (2002) Denaturant dependence of equilibrium unfolding intermediates and denatured state structure of horse ferricytochrome *c*, *J. Biol. Inorg. Chem. 7*, 909−916.
42. Assfalg, M., Bertini, I., Dolfi, A., Turano, P., Mauk, A. G., Rosell, F. I., and Gray, H. B. (2003) Structural model for the alkaline form of ferricytochrome *c*, *J. Am. Chem. Soc. 125*, 2913−2922.
43. Rosell, F. I., Harris, T. R., Hildebrand, D. P., Döpner, S., Hildebrandt, P., and Mauk, A. G. (2000) Characterization of an alkaline transition intermediate stabilized in the Phe82Trp variant of yeast iso-1-cytochrome *c*, *Biochemistry 39*, 9047−9054.
44. Berghuis, A. M., and Brayer, G. D. (1992) Oxidation state-dependent conformational changes in cytochrome *c*, *J. Mol. Biol. 223*, 959−976.

BI0524971